Microfluidic Flow-Flash: Method for Investigating Protein Dynamics

Michael W. Toepke,[†] Scott H. Brewer,[‡] Dung M. Vu,[‡] Kirk D. Rector,[‡] Joel E. Morgan,[§] Robert B. Gennis,[‖] Paul J. A. Kenis,*,[†] and R. Brian Dyer*,[‡]

Department of Chemical and Biomolecular Engineering and Department of Biochemistry, University of Illinois at Urbana−Champaign, Urbana, Illinois 61801, Chemistry Division, Los Alamos National Laboratory, Group PCS, MS J567, Los Alamos, New Mexico 87545, and Department of Biology, Rensselaer Polytechnic Institute, Troy, New York 12180

We report a new method, microfluidic flow-flash, for measuring protein reaction kinetics. The method couples a microscope imaging detection system with a microfluidic flow cell to reduce data acquisition times and sample consumption. This combination allows for the simultaneous collection of spectral and temporal information. The microfluidic flow cell design utilizes three-dimensional sheath flow to reduce sample dispersion and minimize sample consumption. The ability to alter the flow rates in the microfluidic flow cells allows a variety of time scales to be studied with submillisecond time resolution. The imaging detection system can be coupled with several spectroscopic probes including fluorescence and UV/ visible absorbance spectroscopy. Here, we utilize the microfluidic flow-flash method to probe the kinetics of CO recombination or O_2 binding to myoglobin after the laser-induced photolysis of CO from myoglobin by UV/visible absorbance spectral imaging.

Protein dynamics provide the link between the structure and function of a protein. Despite their importance, the functional dynamics of many proteins are poorly characterized due to their complexity and experimental limitations. Protein dynamics span multiple length and time scales; thus, multiple structural probes are often required to fully characterize them. The rapid mixing techniques commonly used to study these dynamics have serious limitations such as large sample requirements and insufficient time resolution. The study of irreversible reactions of proteins and enzymes is particularly hampered by large sample requirements. Thus, methods for studying protein dynamics should include the ability to rapidly initiate and probe protein dynamics over multiple time scales, with sufficient temporal resolution and structural specificity, while minimizing sample consumption. A variety of spectroscopic methods that exhibit only some of the above characteristics have been employed to study a wide range of protein dynamics such as protein folding[1–4] and enzyme reactions.[5–9] Here, we report a new approach to the study of protein dynamics, microfluidic flow-flash, that minimizes sample requirements, covers a broad range of reaction times, and can be coupled with multiple spectroscopic probes.

Microfluidics have been coupled with a variety of spectroscopic techniques to study protein dynamics. These experiments have demonstrated reduced sample consumption[10] and the ability to observe submillisecond events.[11–13] Several spectroscopic probes have been used to perform kinetic studies with microfluidic devices including fluorescence,[10,14–17] FT-IR,[18–21] and NMR.[22] Microfluidic devices can be used to probe the time evolution of a reaction along the flow direction.[10,23] UV/visible absorbance

* To whom correspondence should be addressed. E-mail: bdyer@lanl.gov. Phone: (505) 667-4194. Fax: (505) 667-0440. E-mail: kenis@uiuc.edu. Phone: (217) 265-0523. Fax: (217) 333-5052.
  † Department of Chemical and Biomolecular Engineering, University of Illinois at Urbana−Champaign.
  ‡ Los Alamos National Laboratory.
  § Rensselaer Polytechnic Institute.
  ‖ Department of Biochemistry, University of Illinois at Urbana−Champaign.

(1) Gilmanshin, R.; Williams, S.; Callender, R. H.; Woodruff, W. H.; Dyer, R. B. *Proc. Natl. Acad. Sci. U.S.A.* **1997**, *94*, 3709−3713.
(2) Brewer, S. H.; Vu, D. M.; Tang, Y. F.; Li, Y.; Franzen, S.; Raleigh, D. P.; Dyer, R. B. *Proc. Natl. Acad. Sci. U.S.A.* **2005**, *102*, 16662−16667.
(3) Kubelka, J.; Eaton, W. A.; Hofrichter, J. *J. Mol. Biol.* **2003**, *329*, 625−630.
(4) Roder, H.; Maki, K.; Cheng, H.; Shastry, M. C. R. *Methods* **2004**, *34*, 15−27.
(5) Greenwood, C.; Gibson, Q. H. *J. Biol. Chem.* **1967**, *242*, 1782−1787.
(6) Van Eps, N.; Szundi, I.; Einarsdottir, O. *Biochemistry* **2003**, *42*, 5065−5073.
(7) Sucheta, A.; Georgiadis, K. E.; Einarsdottir, O. *Biochemistry* **1997**, *36*, 554−565.
(8) Sucheta, A.; Szundi, I.; Einarsdottir, O. *Biochemistry* **1998**, *37*, 17905−17914.
(9) Bailey, J. A.; James, C. A.; Woodruff, W. H. *Biochem. Biophys. Res. Commun.* **1996**, *220*, 1055−1060.
(10) Hertzog, D. E.; Michalet, X.; Jaeger, M.; Kong, X.; Santiago, J. G.; Weiss, S.; Bakajin, O. *Anal. Chem.* **2004**, *76*, 7169−7178.
(11) Brody, J. P.; Yager, P.; Goldstein, R. E.; Austin, R. H. *Biophys. J.* **1996**, *71*, 3430−3441.
(12) Knight, J. B.; Vishwanath, A.; Brody, J. P.; Austin, R. H. *Phys. Rev. Lett.* **1998**, *80*, 3863−3866.
(13) Regenfuss, P.; Clegg, R. M.; Fulwyler, M. J.; Barrantes, F. J.; Jovin, T. M. *Rev. Sci. Instrum.* **1985**, *56*, 283−290.
(14) Seong, G. H.; Heo, J.; Crooks, R. M. *Anal. Chem.* **2003**, *75*, 3161−3167.
(15) Benninger, R. K. P.; Hofmann, O.; McGinty, J.; Requejo-Isidro, J.; Munro, I.; Neil, M. A. A.; de Mello, A. J.; French, P. M. W. *Opt. Express* **2005**, *13*, 6275−6285.
(16) Burke, B. J.; Regnier, F. E. *Anal. Chem.* **2003**, *75*, 1786−1791.
(17) Song, H.; Ismagilov, R. F. *J. Am. Chem. Soc.* **2003**, *125*, 14613−14619.
(18) Hinsmann, P.; Haberkorn, M.; Frank, J.; Svasek, P.; Harasek, M.; Lendl, B. *Appl. Spectrosc.* **2001**, *55*, 241−251.
(19) Kakuta, M.; Hinsmann, P.; Manz, A.; Lendl, B. *Lab Chip* **2003**, *3*, 82−85.
(20) Kauffmann, E.; Darnton, N. C.; Austin, R. H.; Batt, C.; Gerwert, K. *Proc. Natl. Acad. Sci. U.S.A.* **2001**, *98*, 6646−6649.
(21) Herzig-Marx, R.; Queeney, K. T.; Jackman, R. J.; Schmidt, M. A.; Jensen, K. F. *Anal. Chem.* **2004**, *76*, 6476−6483.
(22) Kakuta, M.; Jayawickrama, D. A.; Wolters, A. M.; Manz, A.; Sweedler, J. V. *Anal. Chem.* **2003**, *75*, 956−960.
(23) Song, H.; Tice, J. D.; Ismagilov, R. F. *Angew. Chem., Int. Ed.* **2003**, *42*, 768−772.

spectroscopy has not yet been utilized to obtain kinetic data in microfluidic channels, due largely to the longer path lengths that are typically needed to surpass the detection limit.[24] Several techniques have been used to provide sufficient path lengths to acquire absorbance data such as total internal reflection,[25–27] observation along the direction of flow,[28] and larger channels.[29] The manner by which these techniques extend the path length precludes their ability to use convection along the channel to obtain time resolution. Clearly a different approach is required to follow reaction kinetics in a microfluidic cell using UV/visible absorbance spectroscopy.

Dispersion of the sample flow in microfluidic devices has to be considered when using these devices to obtain kinetic information. Segmented flow has been employed previously to eliminate sample dispersion within reacting liquid volumes in microfluidic channels.[17,30] The discrete droplets formed in segmented flow are sufficient for achieving millisecond time resolution; however, observing submillisecond kinetics with this approach is not usually possible due to the technique's mixing time and the challenges related to further downscaling the discrete droplets' volumes.[17] Alternatively, multilayer laminar flow can be used to overcome dispersion by hydrodynamically focusing the analyte to the center of the channel where the velocity distribution is minimal. Sheath flow has already been used in microfluidics to achieve rapid diffusion,[11,12,31,32] direct sample toward surface sensors,[33] prevent sample adhesion to surfaces,[34] focus cells in cytometers,[35,36] and form fibers and tubes.[37] Three-dimensional (3D) sheath flow has also been used to control the cross section and location of the sample stream by varying the relative flow rates of buffer and sample.[38–40]

Flow-flash experiments have a long history of usefulness in studying protein dynamics.[5,41] Flow-flash experiments typically involve the photolysis of CO from a heme protein followed by the irreversible binding of oxygen and any other subsequent reactions.[5–9,42,43] This type of experiment is performed by binding

CO to the protein in a buffer that has been deoxygenated. This solution is then mixed with an oxygenated buffer in the dark. Immediately following mixing, the CO is photolyzed from the protein by a light source to allow oxygen binding to occur. The solutions must be mixed in the dark to prevent loss of CO prior to the laser-induced photolysis, and the mixing time must be faster than the autoxidation time[44] of the protein of interest. The spectrum (typically a UV/visible absorbance spectrum) corresponding to a single time point before or after laser-induced photolysis can be measured for each laser flash, or the time course can be measured at a single wavelength for a single laser pulse. Fresh protein sample is then required to obtain each additional time-resolved spectrum or single-wavelength kinetic trace. New sample is also required to repeat the data measurements to obtain the desired signal-to-noise ratio. Consequently, these experiments typically require a large sample quantity.

Here, we demonstrate the use of a microfluidic flow cell coupled with a microscope imaging system and a CCD array detector to obtain simultaneously full spectral and temporal information (with submillisecond time resolution) for reversible and irreversible reactions while significantly reducing sample requirements. We report microfluidic flow-flash experiments that monitor the recombination of CO or binding of oxygen to myoglobin following laser-induced CO photolysis using UV/visible absorbance spectral imaging. The microfluidic flow cell uses a 3D sheath flow around the sample stream to minimize sample dispersion and sample consumption. The hydrodynamic focusing of the sample stream allows CO or oxygen in the sheath flow buffer to diffuse into the sample stream prior to laser photolysis. The minimal diffusional path lengths resulting from the hydrodynamic focusing minimizes protein autoxidation by limiting the time the protein is exposed to oxygen prior to initiation of the reaction by laser-induced CO photolysis. This method utilizes multichannel UV/visible absorbance detection, covers multiple time scales, minimizes sample consumption, and utilizes rapid laser initiation of the reaction.

MATERIALS AND METHODS

Sample Preparation. Horse heart myoglobin (500–750 μM; Sigma, St. Louis, MO) in 100 mM sodium phosphate buffer (pH 7) was reduced with either sodium dithionite or sodium ascorbate and then exposed to CO gas to form carbonmonoxymyoglobin (MbCO). The buffer for the CO recombination experiments was deoxygenated using excess sodium dithionite and saturated with CO by bubbling the solution with the gas. The buffer for the oxygen binding experiments was saturated with oxygen by bubbling the buffer with oxygen gas. The europium-doped microspheres (40-nm diameter, Molecular Probes (Invitrogen, Carlsbad, CA)) were diluted in 100 mM sodium phosphate buffer (pH 7) to yield a concentration of 0.05–0.1% (w/v) microspheres.

Microfluidic Flow Cell. The microfluidic flow cell was fabricated in poly(dimethylsiloxane) (PDMS) using standard soft lithography methods.[45,46] The bottom layer of PDMS was 1 mm

(24) Verpoorte, E. *Lab Chip* **2003**, *3*, 42N-52N.

(25) Verpoorte, E.; Manz, A.; Luedi, H.; Bruno, A. E.; Maystre, F.; Krattiger, B.; Widmer, H. M.; Van der Schoot, B. H.; De Rooij, N. F. *Sens. Actuators, B* **1992**, *6*, 66–70.

(26) Salimi-Moosavi, H.; Jiang, Y.; Lester, L.; McKinnon, G.; Harrison, D. J. *Electrophoresis* **2000**, *21*, 1291–1299.

(27) Llobera, A.; Wilke, R.; Buettgenbach, S. *Lab Chip* **2005**, *5*, 506–511.

(28) Mogensen, K. B.; Petersen, N. J.; Hubner, J.; Kutter, J. P. *Electrophoresis* **2001**, *22*, 3930–3938.

(29) Srinivasan, V.; Pamula, V. K.; Fair, R. B. *Anal. Chim. Acta* **2004**, *507*, 145–150.

(30) Gunther, A.; Khan, S. A.; Thalmann, M.; Trachsel, F.; Jensen, K. F. *Lab Chip* **2004**, *4*, 278–286.

(31) Tokimoto, T.; Tsukahara, S.; Watarai, H. *Langmuir* **2005**, *21*, 1299–1304.

(32) Tokimoto, T.; Tsukahara, S.; Watarai, H. *Chem. Lett.* **2003**, *32*, 940–941.

(33) Hofmann, O.; Niedermann, P.; Manz, A. *Lab Chip* **2001**, *1*, 108–114.

(34) Munson, M. S.; Hasenbank, M. S.; Fu, E.; Yager, P. *Lab Chip* **2004**, *4*, 438–445.

(35) Yang, R.; Feeback, D. L.; Wang, W. *Sens. Actuators, A* **2005**, *A118*, 259–267.

(36) Seamer, L. C.; Kuckuck, F.; Sklar, L. A. *Cytometry* **1999**, *35*, 75–79.

(37) Jeong, W.; Kim, J.; Kim, S.; Lee, S.; Mensing, G.; Beebe, D. J. *Lab Chip* **2004**, *4*, 576–580.

(38) Nieuwenhuis, J. H.; Bastemeijer, J.; Sarro, P. M.; Vellekoop, M. J. *Lab Chip* **2003**, *3*, 56–61.

(39) Zarrin, F.; Dovichi, N. J. *Anal. Chem.* **1985**, *57*, 2690–2692.

(40) Sundararajan, N.; Pio, M. S.; Lee, L. P.; Berlin, A. A. *J. Microelectromech. Syst.* **2004**, *13*, 559–567.

(41) Gibson, Q. H.; Greenwood, C. *Biochem. J.* **1963**, *86*, 541–554.

(42) Orii, Y. *J. Biol. Chem.* **1984**, *259*, 7187–7190.

(43) Hill, B. C.; Greenwood, C. *Biochem. J.* **1984**, *218*, 913–922.

(44) Brantley, R. E.; Smerdon, S. J.; Wilkinson, A. J.; Singleton, E. W.; Olson, J. S. *J. Biol. Chem.* **1993**, *268*, 6995–7010.

(45) Duffy, D. C.; McDonald, J. C.; Schueller, O. J. A.; Whitesides, G. M. *Anal. Chem.* **1998**, *70*, 4974–4984.

(46) Xia, Y.; Whitesides, G. M. *Angew. Chem., Int. Ed.* **1998**, *37*, 550–575.
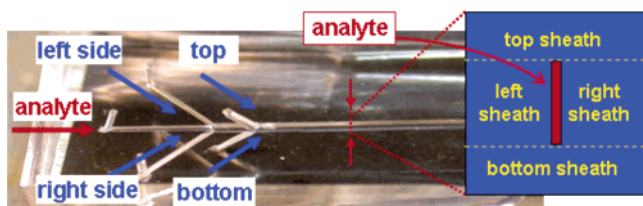
Figure 1. Optical micrograph of the microfluidic flow cell used to create 3D sheath flow for the microfluidic flow-flash experiments. The cell is approximately 2 cm wide and 5 cm long with an observation channel that has a width of 672 μm, a height of 682 μm, and a length of 3 cm.

thick or less, in order to ensure that the center of the channel was within the microscope objective's working distance. The observation channel had a width of 672 μm, a height of 682 μm, and a length of 3 cm. The microfluidic cell design consisted of an inlet region with five flow streams and a long observation channel, as shown in Figure 1. The sample stream (MbCO or europium-doped microspheres) was fed into the flow cell at a rate of 15–25 μL/min using a syringe pump (Harvard Apparatus, Holliston, MA). A gastight syringe (Hamilton, Reno, NV) and capillary PEEK tubing (Upchurch Scientific, Oak Harbor, WA) were used in order to prevent oxygen from reaching the MbCO sample. The sample stream was hydrodynamically focused in the horizontal plane using two buffer streams. Buffer streams were also introduced on the top and bottom of the sample stream several millimeters down the channel to produce a three-dimensional sheath flow with the sample as its inner core.

Detection System. The microscope imaging system consisted of a Carl Zeiss Axiovert 135TV inverted microscope with a 10× or 40× air objective. A halogen or xenon arc lamp (XBO 75, Carl Zeiss, Thornwood, NY) was used to illuminate the sample, and the white light was dispersed by a broadband grating (HVG-590, Kaiser Optical Systems, Ann Arbor, MI) in a 0.25-m imaging spectrograph (Kaiser Optical Systems, Inc.) and imaged by a thermoelectric cooled CCD array detector (PIXIS 400B, 1340 × 400 array, 100-kHz or 2-MHz digitization rates, Princeton Instruments, Trenton, NJ). The microscope imaging detection system can be used to collect fluorescent emission, Raman scattering, and UV/visible absorbance spectral images. In order to acquire spectral and temporal information simultaneously, the flow dimension of the microfluidic flow cell was oriented parallel to the long dimension of the spectrometer slit and the laser excitation source was line focused perpendicular to the flow dimension. This orientation allowed 400 time-resolved spectra to be collected each with 1340 spectral pixels within a single image.

Fluorescent Lifetime Experiments. The fluorescent lifetime of the europium-doped microspheres was used to calibrate the flow rates in the microfluidic flow cell. The europium-doped microspheres in the sample core flow surrounded by a 3D sheath flow of buffer (100 mM sodium phosphate, pH 7) were transiently excited by a CW Coherent Cube laser (405 nm, 10–50 mW; Santa Clara, CA) line focused normal to the flow axis in the microfluidic flow cell. The microscope imaging system described above was used to record a spectral image of the fluorescent decay of the europium-doped microspheres as the microspheres flowed out of the laser excitation volume. These fluorescent images were compared to conventional fluorescence lifetime measurements of

the europium-doped microspheres to determine the flow rate in the microfluidic flow cell. The fluorescent lifetime was determined independently, by transiently exciting the europium-doped microspheres with a frequency-tripled Q-switched Nd:YAG laser (355 nm, 100–900 mW, 10-Hz repetition rate, 10-ns pulse width; Quanta-Ray DCR-5, Spectra-Physics, Mountain View, CA) in a 1-cm-path length cuvette. The fluorescence decay was monitored by a PMT detector attached to a Spex 1681 monochromator to allow only ~610-nm radiation to impinge on the detector. The signal was digitized at 20 MHz.

Microfluidic Flow-Flash Experiments. The sample core flow was MbCO surrounded by a sheath flow buffer saturated with either CO or O_2. A 514.5-nm laser line focus of a CW argon ion laser (1–40 mW; Spectra-Physics, Mountain View, CA) normal to the flow axis of the microfluidic flow cell was used to photolyze CO from Mb. Depending on the dissolved gas in the buffer sheath flow, either CO recombination or O_2 binding followed photolysis. Before photolysis, the dissolved gases in the buffer sheath flows were allowed to diffuse into the sample core flow. The resulting UV/visible absorbance spectral image included spectra before and after the laser line focus corresponding to the protein spectra before and after photolysis. The volumetric flow rate of the solutions, along with the channel dimensions, led to a maximum linear flow rate of 2–7 cm/s at the center of the channel depending on the exact flow rates used in the experiments. The linear flow rates were determined experimentally using europium-doped microspheres with a known fluorescent lifetime (see below) and confirmed by 3D finite element method simulations (Comsol, Multiphysics 3.2, Burlington, MA). The spectral images typically were the result of 8–24 coadds with integration times ranging from 0.1 to 4 s. The images were collected using custom-written LabVIEW (National Instruments, Austin, TX) software and processed using IGOR Pro (WaveMetrics, Portland, OR). Singular value decomposition (SVD) was used to remove some of the noise from the UV/visible spectral images. Each of the SVD components containing signal was used to reconstruct the spectral images. The time-resolved spectra were compared to equilibrium UV/visible difference spectra recorded on a Perkin-Elmer UV/visible spectrometer. The equilibrium difference spectra were obtained by subtracting the absorbance spectrum of MbCO from the absorbance spectra of deoxy-Mb or oxy-Mb. The absorbance spectra were normalized to the Soret band absorbance prior to subtraction.

RESULTS AND DISCUSSION

We have used the microfluidic flow-flash method to study the recombination of CO or the binding of oxygen to Mb after laser-induced CO photolysis from Mb. This method couples a microfluidic flow cell with a microscope imaging detection system. The method utilizes a 3D sheath flow of buffer around the sample stream in a microfluidic flow cell to minimize sample dispersion and sample consumption. The sample stream is interrogated by UV/visible absorbance or fluorescence spectroscopic probes. UV/visible absorbance spectral imaging is used with MbCO as the sample stream for the microfluidic flow-flash experiments while fluorescence imaging is used for the calibration of the flow rates using europium-doped microspheres. One spectral image using the microfluidic flow cell that contains 1340 spectral pixels and 400 time points requires only ~69 pmol of protein sample based

on a 2-MHz digitization rate of the CCD array, 0.1-s integration time, 750 μM protein concentration, and a protein flow rate of 15 μL/min. This sample consumption rate can be further minimized by digitizing a smaller region of the CCD array detector. In contrast, flow-flash experiments using a microcuvette (80-μL volume) require ~256 nmol of protein sample to obtain spectra at 400 time points with a protein concentration of 8 μM.[47] This significant decrease in sample consumption using the microfluidic flow cell permits the study of proteins and especially mutants of these proteins that are difficult or expensive to purify in large quantities.

The time resolution of this microfluidic flow-flash method is defined by the spatial resolution and the flow rate, since each pixel row of the CCD array detector records a spectrum for a single time point. Therefore, the time resolution will improve with smaller spatial resolution elements and faster flow rates. The confocal nature of the detection system should provide optimum spatial resolution, approaching the Rayleigh limit. In principle, this method can achieve <10-μs time resolution. For instance, a 40$\times$ microscope objective and 20-μm detector pixel size yield a 0.5-μm spatial resolution element. This spatial resolution element combined with a linear flow rate of 10 cm/s produces a time resolution of 5 μs based upon a one pixel instrument response time. Higher objective magnifications and faster flow rates can be used to achieve even better time resolution with an optimal laser line focus of the pump beam. The inherent limit to the time resolution is the Rayleigh limit of the laser focus, although sample dispersion may ultimately limit the time response.

The actual time resolution achieved in the experiments reported here is about 1 order of magnitude worse (~50 μs) than the theoretical optimum. This difference is due to two known problems. The first problem is related to the collinear pump and probe beam focusing geometry that does not allow for the independent focusing of each one. Thus, it is difficult to achieve the optimal focus of both beams simultaneously. It should be possible to overcome this limitation by arranging the pump and probe beams orthogonal to one another and to the flow axis. The second problem is inherent to transmission measurements using a microscope having a high numerical aperture objective and probe light that is not fully parallel to the optic axis. Such an optical arrangement results in a sharp focal plane, with a strongly diverging probe beam above and below that plane. The optimum spatial (and temporal) resolution is achieved if the sample stream is hydrodynamically focused to a thickness (the path length of the sample along the optical path of the probe beam) that matches the depth of focus of the probe beam (~10 μm in our experiments). If the sample stream is significantly thicker than the probe beam focal plane, then the diverging probe beam will sample a wider range of the flow stream along the flow direction, thus smearing out the time response. The thickness of the sample stream is controlled in the microfluidics cell by hydrodynamically focusing the sample stream using the top and bottom sheath flows. Since the absorbance signal scales directly with the sample thickness, however, a balance must be achieved between signal level and optimum spatial (temporal) resolution. The optimum sample thickness and hence time resolution will be sample

(47) Van Eps, N.; Szundi, I.; Einarsdottir, O. *Biochemistry* **2000**, *39*, 14576–14582.
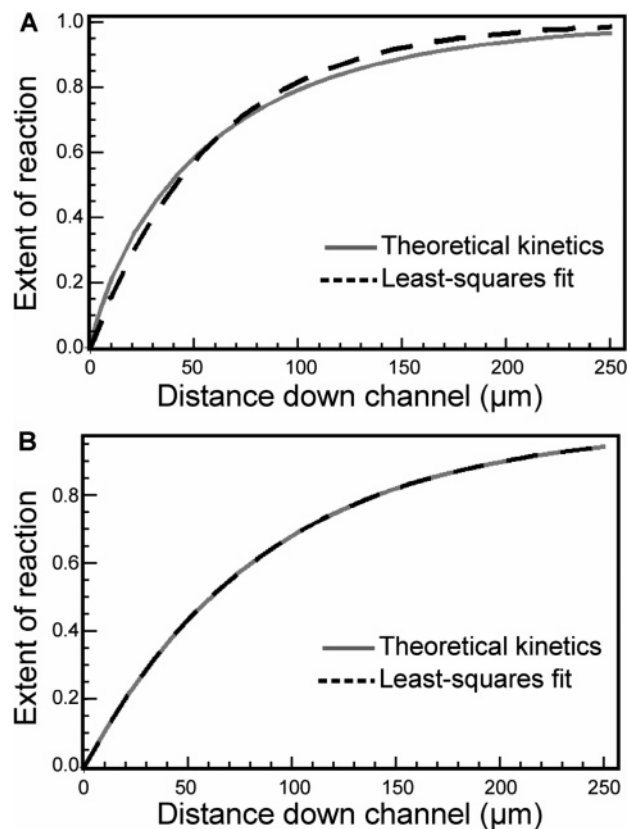
Figure 2. Theoretical effect of parabolic flow on first-order reaction kinetics measured in a microfluidic channel. The calculated extent of reaction (A, solid curve) in the case where parabolic flow results in a distribution of flow rates along the observation direction or (B, solid curve) in the case where parabolic flow is minimized by using 3D hydrodynamic focusing of the sample stream. (The distribution of flow rates was determined for a 20-μm-wide vertical slice at the center of the square microfluidic channel.) The constrained least-square fits (dashed curves in A and B) of the theoretical extents of reaction using a fixed flow rate of 5.7 cm/s and a fixed rate coefficient of 600 s^{-1}.

dependent, varying with concentration, optical density, and the extent of signal averaging. Finally, the effective depth of field of the transmission experiment can be increased using an iris in the probe beam before the sample, so that the light entering the microscope objective is as parallel as possible. We are currently exploring such improvements to determine the best achievable time resolution of our system.

Hydrodynamic Focusing of the Sample Stream. The parabolic nature of pressure-driven laminar flow in microfluidic channels needs be considered when using continuous flow convection to achieve temporal resolution of reaction kinetics since parabolic flow smears out the time dimension. Figure 2A shows the extent of reaction that would be observed along the flow dimension for a first-order reaction if the sample stream is hydrodynamically focused only in the horizontal plane of the microfluidic flow cell (gray curve). This curve accounts for the dispersion of flow rates due to parabolic flow in the plane normal to the flow direction of a 650-μm square channel assuming a first-order rate constant of 600 s^{-1} and a maximum velocity of 5.7 cm/s. This plane is a vertical slice of the cell along the parabolic flow front with a vertical dimension of 650 μm and a width of 20 μm. The dashed black curve shows the first-order least-squares fit to the simulated data (gray curve) using the average linear velocity
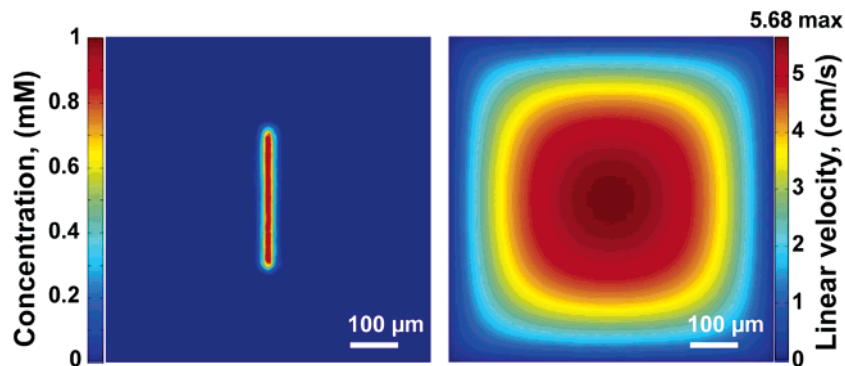
Figure 3. 3D finite element simulation of the velocity and concentration profiles in the microfluidic channel cross section for the conditions used in Figure 2B.

in the channel (Mathematica 3.2, Wolfram Research, Champaign, IL). Neglecting the dispersion within the sample leads to a least-squares fit rate constant for such a system that overestimates the actual rate constant by 15%. Such poor fits can lead to the assumption of incorrect rate laws or large errors in the derived rates.

Three-dimension sheath flow that hydrodynamically focuses the sample stream from the sides and the top and bottom can significantly reduce the dispersion of flow rates resulting from parabolic flow. The 3D sheath flow also reduces sample consumption by forming a sample stream with dimensions much smaller than the microfluidic flow cell dimensions. The sample stream can be hydrodynamically focused so that it just fills the optical slit of the spectrograph to reduce sample consumption further. The top and bottom flows reduce errors from parabolic flow in addition to controlling the sample path length in transmission experiments. The 3D sheath flow decreases diffusional path lengths and thus diffusion times allowing dissolved gases in the sheath flow to diffuse into the sample stream before the observation region of the microfluidic flow cell. The system is run under high Péclet number conditions, so the sample remains concentrated in the center of the channel along the length of the device. Figure 2B shows the theoretical extent of reaction along the flow dimension as for the 3D sheath flow system (gray curve) assuming a first-order rate constant of 600 s^{-1} and an average linear velocity of the analyte of 5.7 cm/s and the least-squares fit curve (dashed black curve) using the average linear velocity in the channel. The introduction of sheath flow both above and below the sample stream reduces the error in the fitted rate constant to less than 1%.

The expected velocity and concentration profiles for the 3D sheath flow system 1 cm from the inlet as determined using 3D finite element method simulations (Comsol Multiphysics 3.2) is shown in Figure 3. These figures are based on the values of the flow rate and rate constant in Figure 2B. For these simulations, the flow rate for the side flows is a factor of 3 greater than the value of the flow rate for the top and bottom flows. Both the concentration and velocity profiles illustrate that the highest concentration and velocity is found at the center of the sample stream and decreases away from the center. Experimentally, the concentration profile aids in helping to find the center of the sample stream where the velocity is at it highest value and is most uniform.
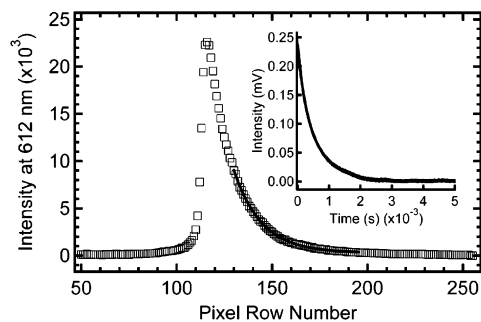
Figure 4. Fluorescent intensity measured at 612 nm of europium-doped microspheres in the microfluidic flow cell before and after being transiently excited by laser excitation (405 nm). Inset: single-wavelength fluorescent lifetime measurement of europium-doped microspheres.
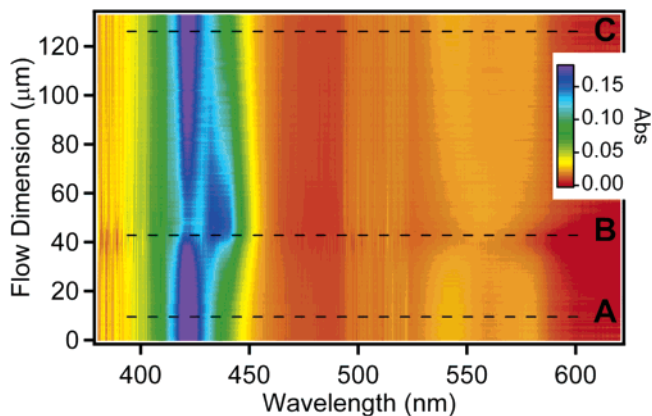
Figure 5. Time-resolved UV/visible absorbance image of CO photolysis and recombination to myoglobin obtained using a microfluidic flow cell. The flow direction is up. Position A is before photolysis, position B is immediately following CO photolysis, and position C is after significant CO recombination.

Calibration of Flow Rates in the Microfluidic Flow Cell.
The calibration of the flow rate and consequently the time axis for the microfluidic flow-flash experiments is performed by using europium-doped microspheres (40 nm in diameter) with a fluorescent lifetime in the hundreds of microseconds. The fluorescent lifetimes of these europium-doped microspheres are first measured independently in a fluorescence lifetime instrument. The fluorescent lifetime decay of the europium-doped microspheres is presented in the inset of Figure 4. The decay is fit to a double-exponential function with lifetimes of 223 and 684 μs.
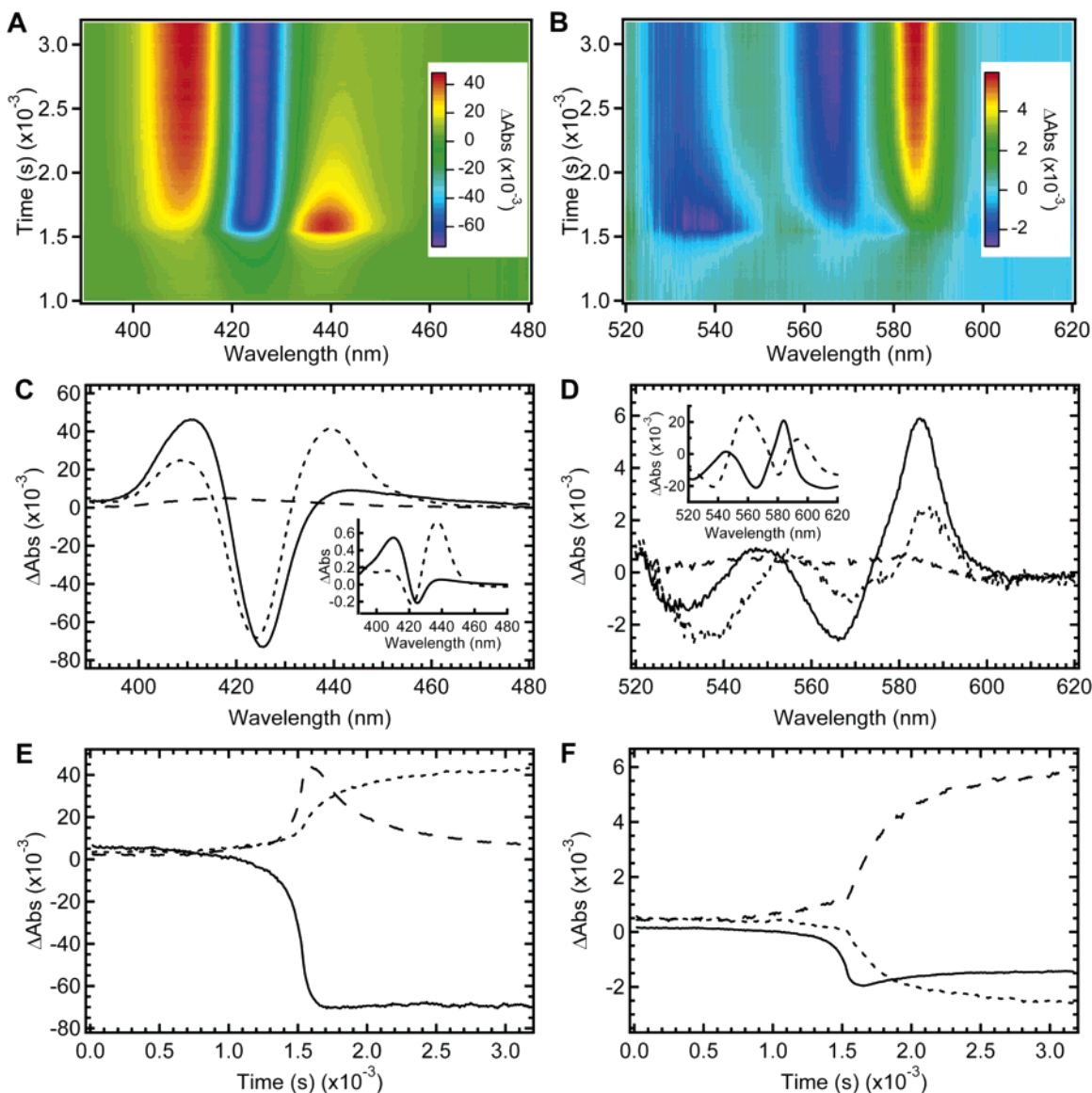
Figure 6. Time-resolved difference UV/visible absorbance images of CO photolysis and oxygen binding to myoglobin obtained using a microfluidic flow cell in the Soret (A) and the α band regions (B). The UV/visible difference spectra of myoglobin corresponding to time points before photolysis (long dashed curve), immediately after photolysis (short dashed curve) and 1 ms after photolysis (solid curve) in the Soret (C) and the α band regions (D) taken from the above images. The kinetic traces at 408 (short dashed curve), 424 (solid curve), 439 nm (long dashed curve) (E), 532 (solid curve), 566 (short dashed curve), and 585 nm (long dashed curve) (F) taken from the above images. Insets: equilibrium difference UV/visible spectra obtained by the subtraction of the MbCO absorbance spectrum from either the deoxy-Mb (dashed curve) or oxy-Mb (solid curve) absorbance spectra.

The slower lifetime contains the largest fraction (0.64) of the total amplitude. The fluorescent lifetime of the europium-doped microspheres using the microfluidic flow cell is then performed using different flow rates and microscope objectives to mimic the microfluidic flow-flash experiments. The europium-doped microspheres are in the core sample flow of the cell surrounded by a 3D sheath buffer (100 mM sodium phosphate buffer (pH 7)) flow. A CW diode laser (405 nm) line focused normal to the flow axis is used to excite transiently the microspheres, while the fluorescence is recorded by the microscope imaging system as the fluorescent microspheres flow in to and out of the laser excitation volume. The resulting kinetic trace at ~612 nm (wavelength of highest fluorescent signal) from the fluorescence image using a $10\times$ microscope objective is shown in Figure 4. The x-axis for Figure 4 corresponds to each pixel row of the CCD array detector.

The fluorescent decay can be fit to a single exponential and this rate constant (pixel^{-1}) along with the predominant fluorescent lifetime of 684 μs is used to calibrate the linear flow rate and hence the time axis in the microfluidic flow cell. Due to the microscope objective and flow rate used to obtain the fluorescent decay shown in Figure 4, only the slower (684 μs) fluorescent lifetime of the europium-doped microspheres is observed.

Flow-Flash Measurements of CO Recombination to Mb. Figure 5 shows a microfluidic flow-flash experiment monitoring the UV/visible absorbance spectra of myoglobin before and after laser-induced photolysis of CO from myoglobin. The sample stream for this experiment is MbCO surrounded by buffer that has been saturated with CO gas. The flow direction is vertical, from the bottom to the top of the image. A laser line focused (514.5 nm) normal to the flow axis was used to photolyze CO from

myoglobin with the flow axis oriented parallel to the long axis of the spectrometer slit. Initially, the absorbance spectra of myoglobin show a Soret peak at 421 nm indicative of MbCO (position A). The Soret maximum shifts to 434 nm after laser photolysis due to the formation of deoxy-Mb (position B). CO and myoglobin then recombine later in time (further along the microfluidic flow cell away from the laser line focus, up in the figure) to return the Soret peak maximum to 421 nm (position C). The distinct α bands for the CO bound Mb at 543 and 579 nm merge after laser photolysis also indicating the formation of deoxy-Mb and subsequently return to the prephotolysis positions downstream from the laser focus due to CO recombination. The time axis (*y*) was not calibrated for this particular data set, but the flow dimension is given in micrometers based on the number of rows of the CCD array and the dimension of each pixel. The initial formation of deoxy-Mb and subsequent recombination of CO are clearly resolved in these experiments. Furthermore, the complete spectral evolution for these processes is captured. The latter feature of this method should prove valuable for analyzing more complex kinetics.

Flow-Flash Measurements of O$_2$ Binding to Mb. Figure 6 shows a microfluidic UV/visible flow-flash experiment monitoring the irreversible binding of oxygen to myoglobin after laser-induced CO photolysis. In this experiment, MbCO is the sample core flow in the microfluidic flow cell surrounded by 3D sheath buffer solution saturated with O$_2$. Prior to laser photolysis, the hydrodynamic focusing of the sample stream allows for the diffusion of the dissolved oxygen from the buffer sheath flows into the central sample stream. While the sample is in the dark, oxygen cannot bind to myoglobin in the limited time before laser photolysis. Following laser-induced CO photolysis, the photolyzed CO concentration will decrease due to diffusion of photolyzed CO into the buffer sheath flows and oxygen binds preferentially to deoxymyoglobin. As with the previous experiments, the flow axis was oriented parallel to the long axis of the spectrometer slit and the laser pump beam used to photolyze CO from Mb was line focused normal to the flow axis. Panels A and B in Figure 6 show the difference UV/visible spectral image resulting from the microfluidic flow-flash experiment. The flow direction in Figure 6A and B is up. These images show the initial laser-induced CO photolysis resulting in the formation of deoxy-Mb and the subsequent formation of oxy-Mb in the Soret (A) and α band spectral regions, respectively. (The data in these figures were obtained simultaneously but are displayed here as separate images for readability, because of the large absorbance differences between the two spectral regions). The difference spectral image is obtained by subtracting the UV/visible absorption image without the laser excitation from an image with the laser excitation impinging on the sample.

The images in Figure 6A and B are analyzed by examining the time-resolved difference UV/visible spectra and the kinetic traces at various wavelengths. Representative spectral slices from the image data of Figure 6A and B are shown in Figure 6C and D. The difference UV/visible spectra of myoglobin before photolysis (long dashed curve), immediately after photolysis (short dashed curve), and 1 ms after photolysis (solid curve) in the Soret and α band region are presented in Figure 6C and D, respectively. The insets of these figures show the equilibrium difference UV/ visible spectra obtained by subtracting the absorbance spectrum of MbCO from the absorbance spectra of either deoxy-Mb (dashed curve) or oxy-Mb (solid curve). A comparison of the time-resolved difference spectra and the static difference spectra confirms the formation of deoxymyoglobin immediately after photolysis, followed by a decrease in deoxymyoglobin as oxygen binds to myoglobin. The decrease in absorbance in Figure 6A (blue band) and C (trough near 424 nm) is due to CO photolysis, while the transient absorbances at 439 and 408 nm are due to the formation of deoxymyoglobin and oxymyoglobin, respectively. Figure 6E shows the initial decrease in absorbance at 424 nm for the photolysis of CO from Mb. In addition, an initial increase in absorbance observed at 439 nm is due to formation of deoxy-Mb. This initial change is followed by an increase in absorbance at 408 nm due to oxygen binding to Mb and a concomitant decrease in absorbance at 439 nm. The rate of oxygen binding is consistent with previous literature values.[9] Figure 6D shows the α band spectral features indicating oxygen binding. Figure 6F shows the kinetic traces for the three dominant features in Figure 6B and D. The kinetic traces at 566 and 585 nm are primarily the result of O$_2$ binding to myoglobin while the trace at 532 nm is the result of the initial formation and subsequent decrease in deoxy-Mb. This trace does not return to the baseline due to contributions from oxymyoglobin at this wavelength.

CONCLUSIONS

The microfluidic flow-flash method was demonstrated by investigating the dynamics of CO recombination or oxygen binding to myoglobin following the laser-induced photolysis of CO from Mb using UV/visible absorbance spectral imaging. This new method combined a microscope imaging detection system with a microfluidic flow cell for the simultaneous collection of spectral and temporal information with submillisecond time resolution while minimizing sample consumption. The ability to collect the full spectral response can be used to sort out complex processes. The microfluidic flow cell utilized a 3D sheath flow to minimize parabolic flow of the sample stream, and the flow rates in the microfluidic flow cell were determined by the fluorescent decay of transiently excited europium-doped microspheres in the sample stream. This method can be extended to other protein systems such as enzymes using either laser initiation or hydrodynamic focusing to produce rapid diffusion of reactants into the sample stream to initiate enzyme reactions.